Thermal Performance of Pulsating Heat Stripes (PHS) Built with Plastic Materials

Oguzhan Der
PhD Candidate
Laboratory of Technical Physics
School of Engineering
University of Liverpool
Liverpool, United Kingdom, L1 5AQ
Email: O.Der@liverpool.ac.uk

Marco Marengo
Professor of Thermal Engineering
School of Computing,
Engineering and Mathematics
University of Brighton
Brighton, United Kingdom, BN2 4GJ
Email: M.Marengo@brighton.ac.uk

Volfango Bertola*
Senior Lecturer in Thermofluids
Laboratory of Technical Physics
School of Engineering
University of Liverpool
Liverpool, United Kingdom, L1 5AQ
Email: Volfango.Bertola@liverpool.ac.uk

A low-cost, flexible pulsating heat pipe (PHP) was built in a composite polypropylene sheet consisting of three layers joint together by selective laser welding, to address the demand of heat transfer devices characterized by low weight, small unit thickness, low cost, and high mechanical flexibility. A thin, flexible and lightweight heat pipe is advantageous for various aerospace, aircraft and portable electronic applications where the device weight and its mechanical flexibility are essential. The concept is to sandwich a serpentine channel, cut out in a polypropylene sheet and containing a self-propelled mixture of a working fluid with its vapour, between two transparent sheets of the same material; this results into a thin, flat enclosure with parallel channels hence the name "pulsating heat stripes" (PHS). The transient and steady-state thermal response of the device was characterised for different heat input levels and different configurations, either straight or bent at different angles. The equivalent thermal resistance was estimated by measuring the wall temperatures at both the evaporator and the condenser, showing a multi-fold increase of the equivalent thermal conductance with respect to solid polypropylene.

Nomenclature

D_H Hydraulic diameter, m
g Gravity, m/s^2
P Pressure, Pa
$\dot{Q}$ Power, W
T Temperature, °C
μ Dynamic viscosity, Pa·s
ρ Density, kg/m^3
σ Surface tension, N/m
τ Deformation stress, Pa

1 Introduction

In the recent years, the pulsating heat pipe (PHP) technology has been the object of intensive investigations because of its potential to meet many of the present and future passive thermal management requirements in several applications, including nuclear, defense and aerospace [1–3]. To date, several PHP designs have been proposed and characterised to address electronics cooling [4, 5], heat recovery [6, 7] and passive cooling of reactor containments, to name a few. However, certain characteristics of state-of-the-art PHPs make their use technically challenging in several cases. This often prevents potential applications to a range of novel consumer technologies, where mechanical flexibility and weight are critical design and/or marketing constraints. For example, flexible devices can be applied in multiple potential configurations, where the heat sink is out of plane with the heat source [8].

Early studies, mainly focusing on space applications, proposed to obtain local flexibility in the adiabatic region using bellowed tubes [9, 10]. More recently, there was an increasing interest in the development of flexible PHP devices built using thin metal foils, sintered metals [11], polymeric materials [12, 13] and micro-machined liquid crystals [14]. However, the approaches proposed so far suffer

*Address all correspondence to this author.

from several technical issues. Firstly, the fabrication of flexible metallic components is possible only using thin-walled tubes and/or thin metal foils, with severe reduction of their mechanical resistance, in particular to fatigue; this has obvious consequence on the system reliability and operational lifetime. Secondly, these flexible heat pipes are not based on the wickless PHP concept, but the liquid phase circulation is promoted by a micro-manufactured wick structure, such as sintered copper woven mesh [13]; this results into high manufacturing cost and poor mechanical strength. Other technical issues encountered were liquid and gas diffusion through the polymer and billowing of the flexible material due to pressure differentials. Very recently, a flexible pulsating heat pipe was fabricated by thermally sintering a multi-layer polymer film including an aluminium layer acting as gas barrier on the two sides of a LDPE sheet cut into a closed-loop PHP shape [15]. To minimize diffusion of non-condensable gases through the seal, an indium coating was deposited on the heat pipe perimeter.

The present work investigates the thermal performance of a flexible, lightweight, low-cost heat pipe technology. The basic concept is to sandwich a serpentine channel, which is cut out in a polypropylene sheet and contains a self-propelled gas-vapour mixture, between two transparent polypropylene sheets bonded together by selective laser welding [16]. The resulting channel has a rectangular cross-section characterized by a large aspect ratio, hence the denomination *Pulsating Heat Stripes* (PHS). Although the diffusion of non-condensable gases through polymer films and sheets represents the main hindrance to the practical applications of polymeric PHPs, because it causes a deterioration of the thermal performance which limits the lifetime of devices, this problem can be addressed independently of the thermal and mechanical characterisation, which is the main focus of this work.

The proposed PHS technology has no equivalent among state-of-the-art commercial or research heat transfer devices, both in terms of thermo-mechanical properties and potential applications. In addition, the proposed device can be seen as a novel type of composite polymeric material with enhanced heat transfer characteristics, and significantly higher equivalent thermal conductivity in comparison with the individual component materials. Perspective applications of PHS effective thermal management of passive nature in entirely new devices and materials, such as fabrics equipped with microelectronic devices, whose thermal management is severely hindered at present by mechanical, size, or weight constraints.

2 PHS Manufacturing

2.1 Materials Selection and Fabrication

The manufacturing process, schematically illustrated in Figure 1a, consists in cutting out a serpentine channel into a black polymer sheet (0.7 mm thickness), which is placed between two transparent sheets of the same material (0.4 mm thickness each). The three polymer sheets are then bonded together by selective laser welding to create a strong and

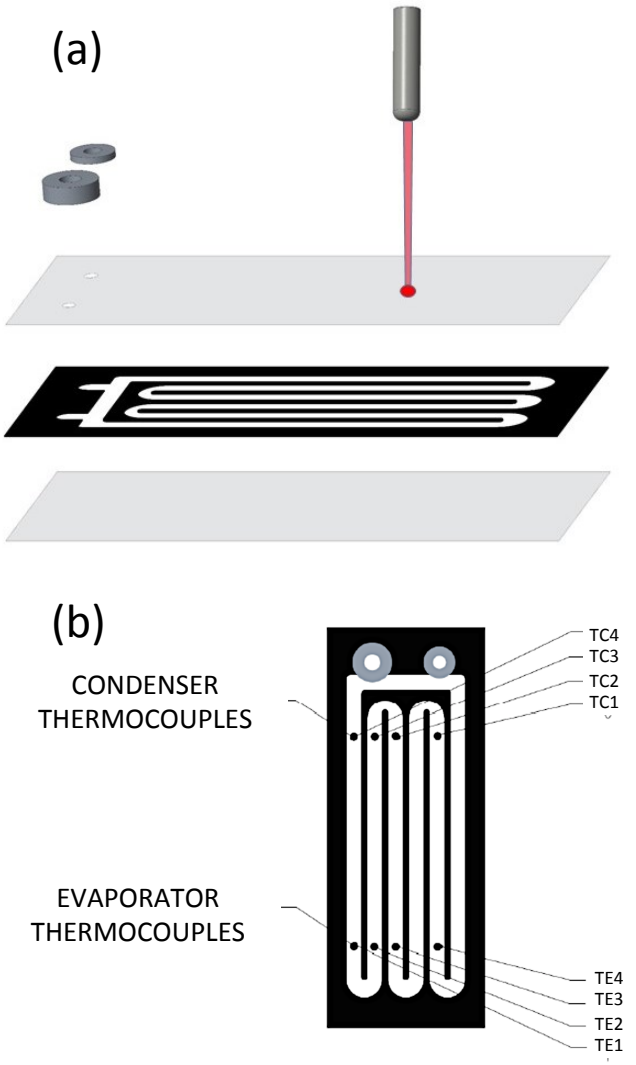

Fig. 1. Schematic of the PHS assembly and laser welding process (a) and top view of the assembled PHS showing the serpentine channel and the location of surface thermocouples (b).

seamless joint among the three sheets; while the external sheets are transparent to the laser wavelength, the central black layer absorbs the same wavelength, to enable polymer bonding exactly at the interface, without affecting the rest of the material [17, 18].

The polymer sheets material (polypropylene) was selected based on: (i) mechanical properties (elastic modulus, yield stress, resistance to fatigue); (ii) compatibility with a range of organic heat transfer fluids (ethanol, acetone, refrigerant fluids); (iii) suitability to laser welding; the maximum continuous service temperature is 130°C. After assembling the three sheets, a PVC block was glued (Loctite All Plastic) in correspondence of two holes in one of the transparent sheets, to fit a pressure transducer and a micro-metering valve used for vacuuming and filling.

The PHS assembly has a length of 250 mm, a width of 98 mm, and a thickness of 1.5, as shown in Figure 1b. The serpentine has six passes (five turns), and the channel cross-section is 9 mm x 0.7 mm, resulting into a nominal hydraulic

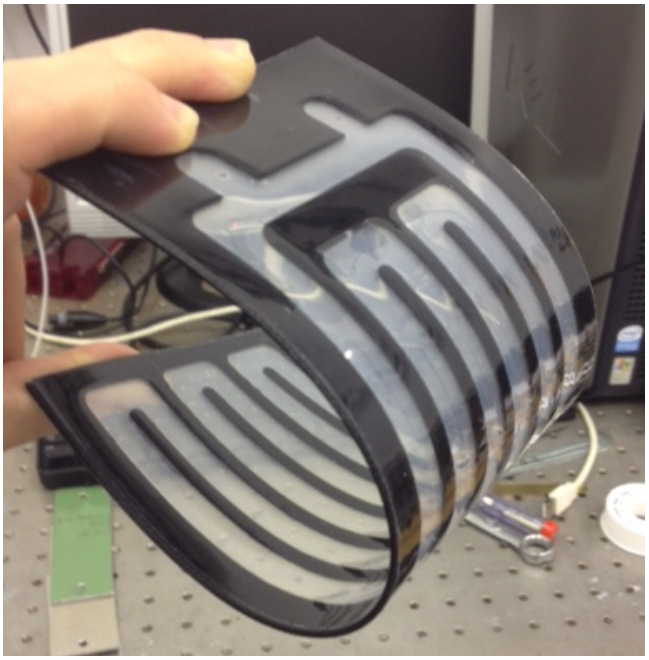

Fig. 2. Demonstration of the PHS flexibility (180° bending).

diameter $D_H = 1.3$ mm. This value satisfies the design criterion given in Eq. (1) to ensure surface forces prevail on gravity [19], using FC-72 ($\rho = 1680$ kg/m^3; σ = 10 mN/m) as working fluid (0.54 mm < 1.3 mm < 1.4 mm).

$$0.7\sqrt{\frac{\sigma}{g(\rho_L-\rho_G)}} \leq D_H \leq 1.8\sqrt{\frac{\sigma}{g(\rho_L-\rho_G)}} \qquad (1)$$

2.2 Mechanical and Hydraulic Performance

Figure 2 demonstrates the mechanical flexibility achieved with the proposed manufacturing technology; the PHS can be bent at an angle of 180°, with a radius of curvature of approximately 30 mm. However, mechanical flexibility also affects the channel walls, which adjust their shape according to the pressure difference between the working fluid and the atmosphere; in particular, channel walls inflate when $P_{fluid} > P_{atm}$, and appear concave when $P_{fluid} < P_{atm}$.

The channel deformation obviously affects the pressure level during the PHS operation, both because of the volume change, and because the pressure difference between the external (atmospheric) and the internal (fluid) pressure must balance the stress that builds up in the deformed channel walls, which acts to recover the initial flat shape (Eq. 2); this is similar to the concept of Laplace pressure across a curved fluid interface.

$$P_{atm} = P_{fluid} \pm \tau_{def} \qquad (2)$$

More importantly, the channel deformation affects the hydraulic diameter since the cross-section of the PHS channels changes depending on the instantaneous pressure level; thus, the hydraulic diameter value may fall outside the optimal range given by Eq. 1, reducing the thermal performance of the device.

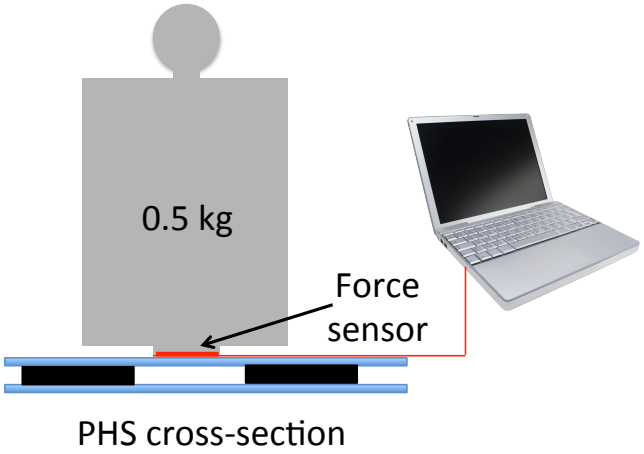

Fig. 3. Schematic of the experimental arrangement to estimate the relaxation stress in the PHS wall.

An additional complication to account for is that in polymeric materials the deformation stress is not constant, but is subject to stress relaxation, i.e., the observed decrease in stress in response to a certain amount of strain generated in the material. This is usually described using either the Maxwell or the Kelvin-Voigt constitutive equation, or a combination of them [20]. Thus, any pressure change in the PHS channel causes a wall deformation, which in turn induces an apparent pressure change consistent with Eq. (2), i.e. to compensate the stress relaxation in the channel wall. The peculiar response of the PHS to internal pressure variations may generate ambiguities in the interpretation of pressure measurements. For example, after vacuum is initially created in the PHS, before filling with the working fluid, one can still observe a slow increase in the absolute pressure, as discussed below. In a conventional PHP with rigid walls, this would indicate with no doubt a leak, however in PHS with flexible walls the apparent pressure change could be also attributed to the channel wall relaxation.

To quantify the relaxation of PHS walls, a calibration weight of 0.5 kg with a base area of 0.5 cm^2 was placed on an empty PHS (i.e., at atmospheric pressure), as shown schematically in Figure 3; in these conditions, the net pressure on the PHS wall is the same as in vacuumed PHS, i.e., approximately one bar. A capacitive force sensor with the same area (SingleTact) was placed between the PHS wall and the weight; in case of a rigid wall, the sensor would measure a constant force, equal to the weight, but if the wall is not rigid the measured force decreases in time due to the relaxation of the material.

Figure 4 displays the relaxation of the measured force during a timespan of 60 hours; the relaxation time of the wall, i.e. the time to reach an approximately constant value, is of the order of 30 hours, after which a residual force of the order of 1.5 N is measured. Such relaxation time is much longer than the typical duration of thermal transients where

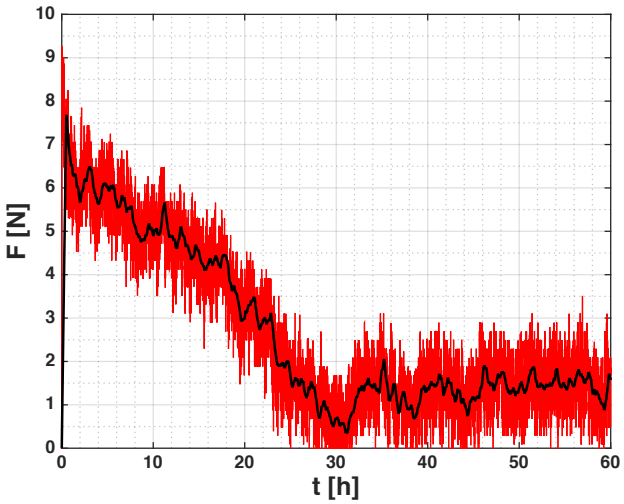

Fig. 4. Force measured by the sensor sandwiched between the weight and the PHS wall (see Figure 3). The black line indicates the moving average over 30 minutes.

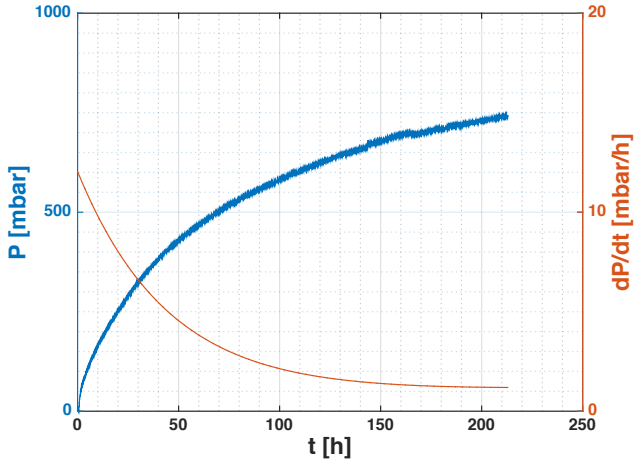

Fig. 5. Pressure variation in the vacuumed PHS (left axis) and corresponding pressure variation (right axis) as a function of time.

the PHS attains a pseudo-steady-state thermohydraulic operating condition, therefore the effects of wall relaxation cannot be neglected.

The absolute pressure measured inside the PHS (without working fluid) and the corresponding pressure gradient are shown as a function of time in Figure 5. The observed pressure increase depends on the permeation of non-condensable gases through the PHS walls and bonds, of potential leaks through the fittings of the micro-metering valve and of the pressure transducer, and of the PHS walls relaxation, as illustrated above.

A detailed analysis of the permeation pressure in a polymeric PHP is reported in Reference [15] based on Fick's law and literature data. As a matter of fact, the gas permeability coefficients used in this analysis depend not only on the type of polymer, but also on the degree of polymerization, on the polymer conformation, on the degree of crystallization, and on the manufacturing process (moulding, extrusion, etc).

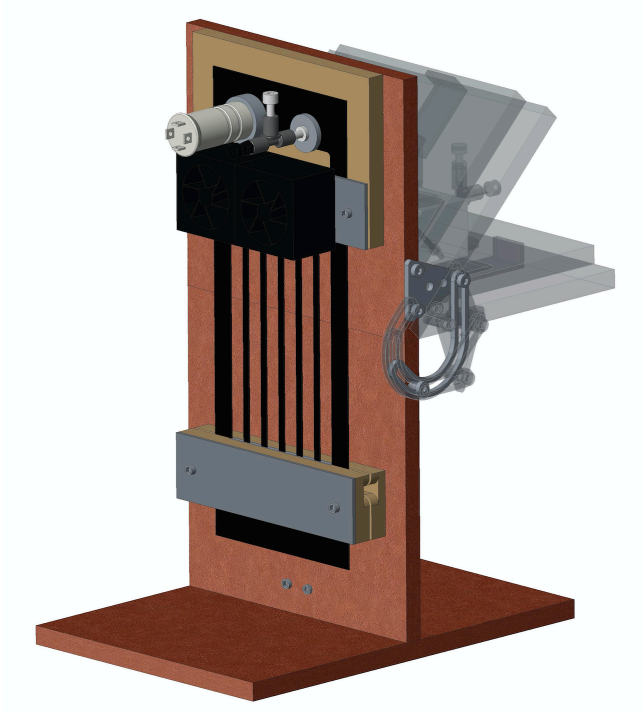

Fig. 6. 3D view of the experimental kit showing the bending mechanism.

Thus, any attempts to predict gas permeation are affected by significant uncertainties, and the only way to obtain realistic data is to carry out direct measurements. At present, the most viable technical solution to reduce gas permeation is the use of metallized polymer sheets. However, a full understanding of the pressure dynamics inside the PHS can be achieved only through comprehensive structural analysis, combined with an analytical and/or experimental quantification of gas permeation through the material and of other potential leaks, which is beyond the scope of the present work.

Whilst the pressure level in the PHS becomes significant in a few days, which prevents the practical use of the device in applications at atmospheric pressure, the pressure gradient (of the order of 1 kPa/h or less) is small enough to enable a complete thermal characterisation experiment, which has a maximum duration of about six hours.

3 Experimental Setup and Procedure

3.1 Experimental Setup

A schematic view of the experimental setup is shown in Figure 6. The PHS units were mounted on a vertical support, with the evaporator zone at the bottom and the condenser at the top. A hinge in the middle of the support plate allowed bending the PHS at different angles between 0° and 90°.

Two ceramic heaters (100 W each) were applied to both sides of the PHS in the evaporator region; heat sink paste was used to minimise the contact resistance and two copper plates having the same width of the PHS were used to distribute the heat supply uniformly. The heaters and the copper plates were housed in a 1 cm thick block of Superwool 607HT (Thermal Ceramics Ltd.), a material with ther-

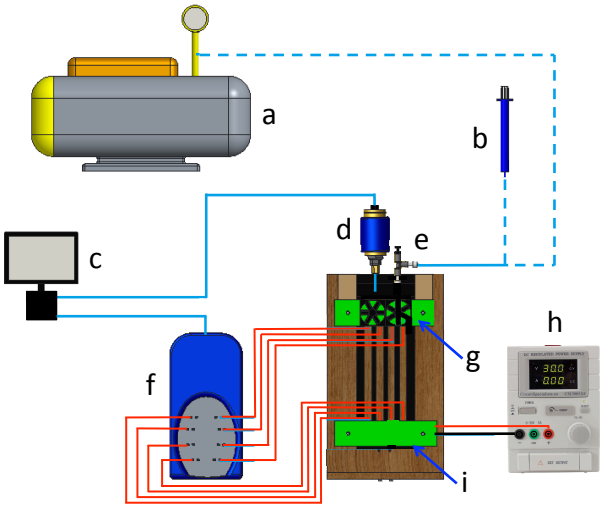

Fig. 7. Schematic of the experimental setup: (a) vacuum pump; (b) syringe; (c) data logger and PC; (d) pressure transducer; (e) micro-metering valve; (f) thermocouples unit; (g) condenser fans; (h) power supply; (i) electric heaters.

mal conductivity ≤ 0.05 W/mK; the assembly was clamped between two 1.5 cm thick timber strips (thermal conductivity: 0.15 W/mK). Thus, the heat loss can be estimated as $q"_{loss} = 3.33(T_{evap} - T_{amb})$ W/m^2, and ranges between 3.5% at maximum power (30 W) and 6.4% at minimum power (5 W). The heaters were connected to a regulated DC power supply (Circuit Specialists CSI 12001X) to enable a fine control of the power input.

In the condenser section, the PHS were clamped between two aluminium plates coated with a thin layer of heat sink paste; two fan-assisted heat sinks (Malico) were mounted on the external plate. The evaporator and the condenser sections had an identical length of 4 cm.

The heat pipe was connected to a pressure transducer (Gems 3500, 0-160 kPa) and to a micro-metering valve (Upchurch Scientific), used in turn to vacuum the PHS and to fill the PHS with the working fluid. The pressure transducer DC output was sampled at 1 Hz by a data acquisition system (LabJack U6).

Eight surface thermocouples (Omega Engineering) with response time ≤ 0.3 s and flat probe junction were securely fastened between the PHS surface and the metal holder after dipping the probes into heat sink paste, four in the evaporator zone and four in the condenser zone, and connected to a data acquisition system. The temperature distribution in the adiabatic region was monitored by a FLIR One infra-red camera (FLIR Systems Inc.). The sensors positions and connections are shown schematically in Figure 7.

3.2 Procedure

The working fluid used in all experiments was Refrigerant FC-72 ($\rho = 1680$ kg/m^3, $\sigma = 10$ mN/m , $\mu = 0.7$ mPa.s at 20°C), de-gassed in a vacuum chamber (Bacoeng) for 24 hours before use. To introduce the working fluid, the PHS modules were vacuumed to a pressure of 0.2 ± 0.5 kPa (abs) using a two-stage vacuum pump (Bacoeng); then, the fluid contained in an external syringe reservoir was slowly driven by the atmospheric pressure into the PHS as the micro-metering valve was gently opened. The amount of working fluid used in the present experiments was 3.4 mL, i.e. 40% of the total PHS volume (8.4 mL). The volumetric filling ratio of 40% was determined based on preliminary tests to ensure a maximum pressure of approximately 1.5 bar (abs).

Experiments were conducted by applying to the evaporator section an ascending/descending stepped power ramp ranging between 5 W and 30 W (in particular, the average heat fluxes at each step were 1303, 2525, 4013, 5780, and 7837 W/m^2), and measuring the temperatures on the PHS surface at a sampling rate of 1 Hz. For each power step, the heat supply was kept constant until a pseudo steady-state regime was attained, which typically required about 45 minutes. Tests were interrupted earlier in case any point of the PHS reached a temperature of 120°C, to avoid polypropylene softening and/or melting. Preliminary experiments [16] showed the start-up of two-phase circulation in the PHS occurs with a heat input of about 2.5 W at the evaporator.

The equivalent thermal resistance of the PHS was calculated as:

$$R = \frac{T_{ev} - T_{cond}}{\dot{Q}} \tag{3}$$

where T_{ev} and T_{cond} are the averages of the four temperature measurements of the PHS surface at the evaporator and the condenser, respectively, in the pseudo steady-states corresponding to each level of the power input, $\dot{Q}$. For the sake of comparison with the thermal resistance of the bare composite polypropylene sheet, one test was carried out using a vaccumed PHS module, without working fluid.

Experiments were carried out for two main PHS configurations: (i) straight arrangement, with vertical, horizontal and 45° orientations, respectively, and (ii) bent at 45° and 90° in the middle of adiabatic zone, with vertical evaporator and inclined/horizontal condenser, respectively. Each test was carried out using a fresh PHS unit to ensure homogeneous experimental conditions.

4 Results

4.1 Straight Arrangement

Examples of FLIR images of the adiabatic region of PHS in straight vertical arrangement during the heating ramp, showing the temperature distributions for three values of the heat supply at the evaporator ($\dot{Q} = 5.2W$, $\dot{Q} = 16W$, and $\dot{Q} = 31.3W$, respectively) are displayed in Figure 8. As the power supply is increased, more channels become active and the heated fluid occupies a longer part of channels. For the lowest heat input (Figure 8a), one can visualize ascending plumes of hot boiling fluid and descending colder condensate in the same channel, while for the highest heat input (Figure 8c) individual channels can be clearly distinguished, with their bottom part containing the boiling fluid and the condensate confined in the upper part.

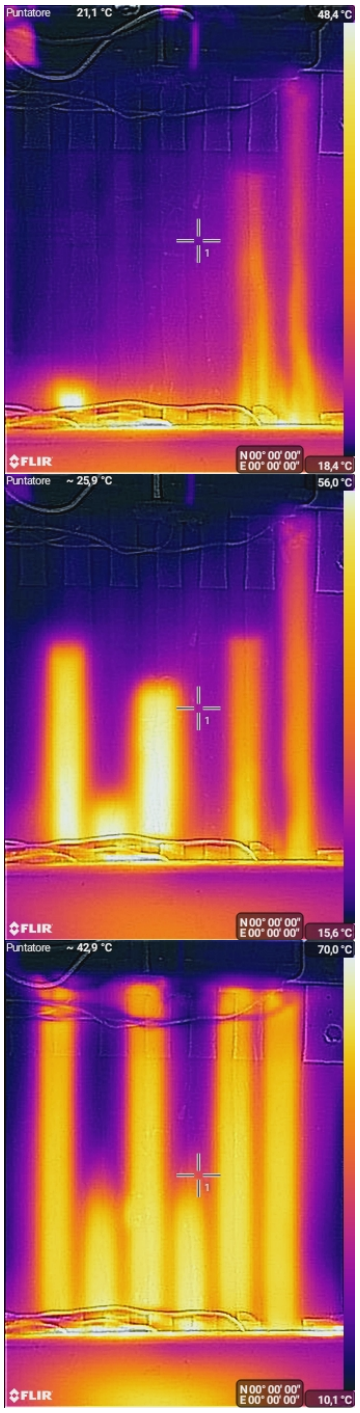

Fig. 8. Examples of FLIR images of the adiabatic region of PHS in straight vertical arrangement during the heating ramp: (a) $\dot{Q} = 5.2W$; (b) $\dot{Q} = 16W$; (c) $\dot{Q} = 31.3W$.

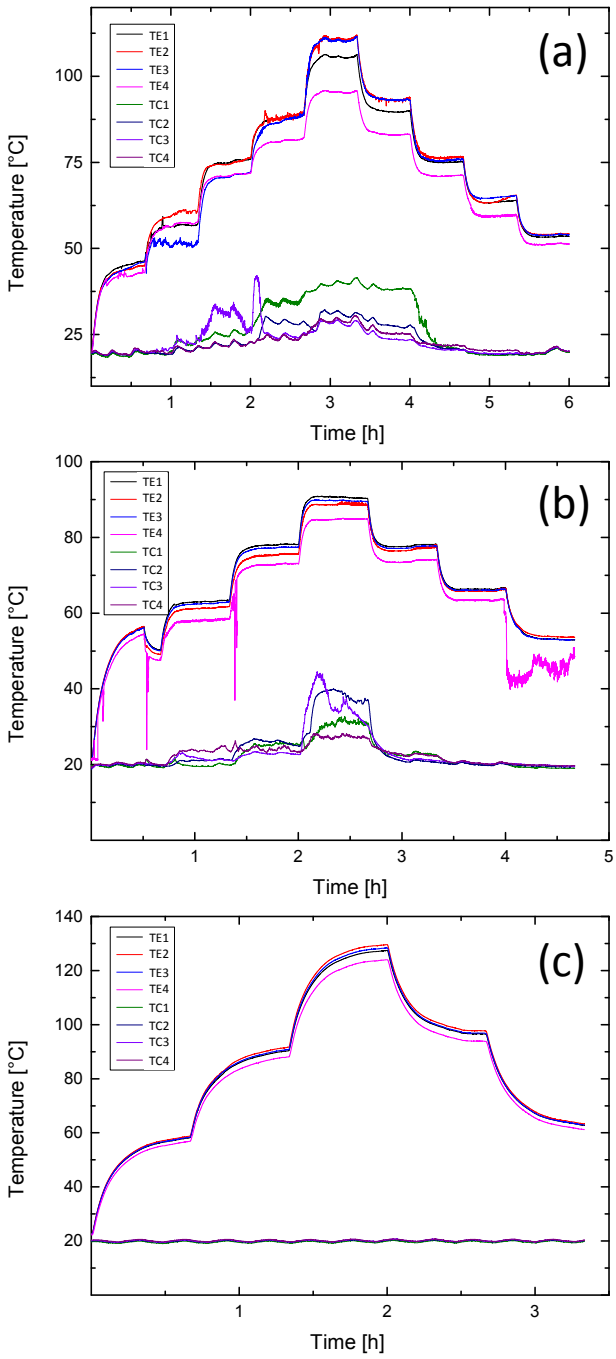

Fig. 9. Temperatures measured in the evaporator ($T_{E1} - T_{E4}$) and in the condenser ($T_{C1} - T_{C4}$) zones of the PHS in straight arrangement during the ascending/descending power supply ramp: (a) vertical; (b) inclined at 45°; (c) horizontal.

Temperatures measured in the evaporator and in the condenser zones of the PHS in straight arrangement during the ascending/descending heat supply ramp are displayed in Figure 9, while the corresponding absolute pressure in the PHS channel is displayed in Figure 10. As expected, both temperatures and pressure exhibit hysteresis, which is partly due to the intrinsic system inertia, partly due to potential leaks and gas permeation, and partly due to the channel wall relaxation discussed in Section 2.2 above. In particular, values of the evaporator temperature hysteresis between the first and the last step of the ascending/descending heat supply ramp are between 2°C and 8°C, while values of the absolute pressure hysteresis inside the PHS are between 75 mbar and 300 mbar. These values are comparable with those obtained from the pressure loss curve at 20°C reported in Figure 5, at times corresponding to the total duration of each test.

The overall thermal performance of the PHS in straight arrangement is shown in Figure 11, which displays the equiv-

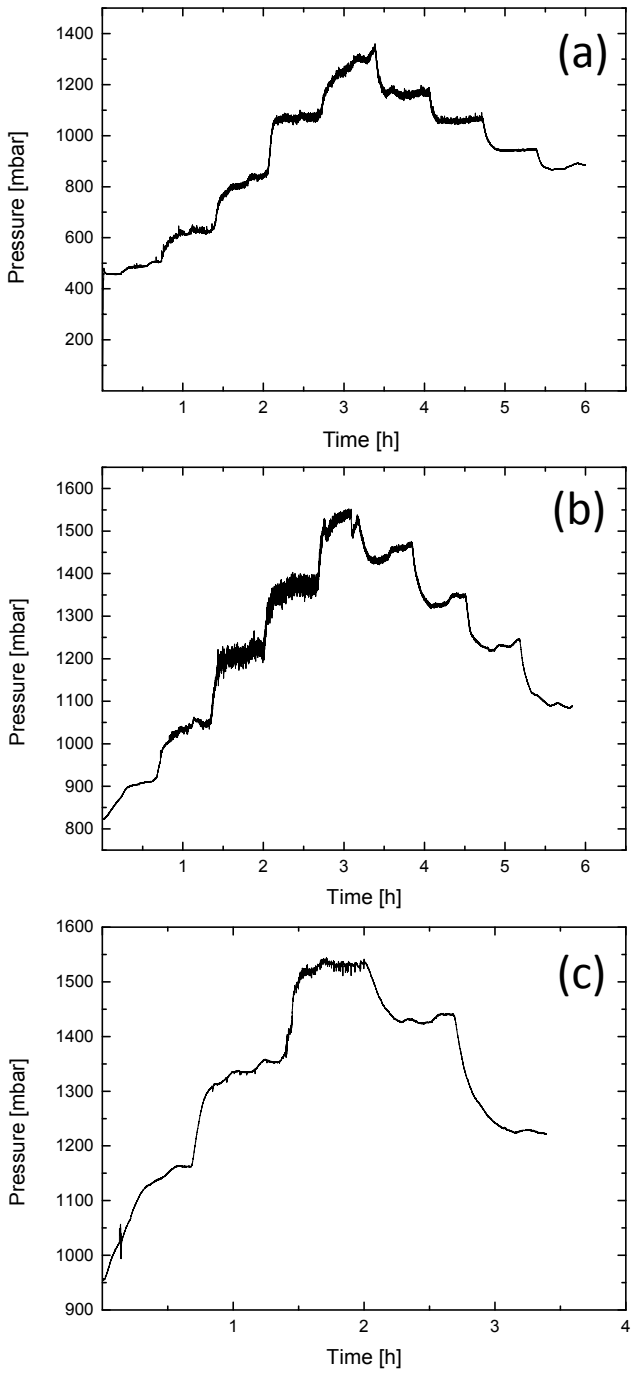

Fig. 10. Absolute pressure measured in the PHS in straight arrangement during the ascending/descending power supply ramp: (a) vertical; (b) inclined at 45°; (c) horizontal.

alent thermal resistance of the PHS at different angles, calculated according to Eq. (3). To estimate the heat transfer enhancement due to the fluid circulation, the equivalent thermal resistance of the vacuumed PHS module without working fluid (R_0=8.87 °C/W) is also displayed.

The lowest value of the equivalent thermal resistance is observed with the PHS module in vertical position at the maximum heat supply of 31.3 W, where it attains a minimum of 2.34 °C/W; this means the equivalent thermal conductance

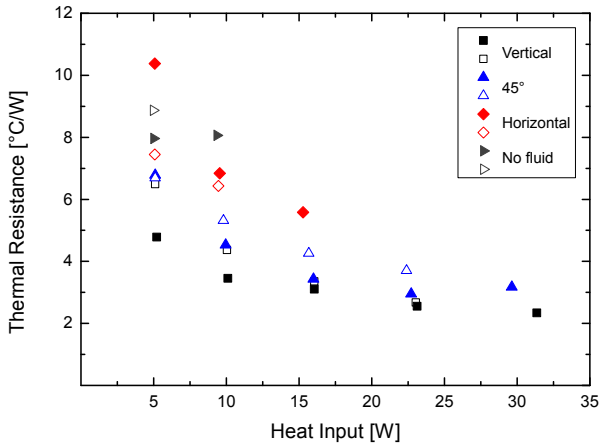

Fig. 11. Equivalent thermal resistance of the PHS in straight arrangement, as a function of the heat rate supplied at the evaporator, for different inclination angles; filled symbols: increasing power; open symbols: decreasing power. The standard deviation based on three tests is $\leq 8\%$.

of the PHS increases of about 400% with respect to the composite polypropylene sheet without working fluid.

Whilst the hydraulic diameter of the PHS channels was designed to ensure the device works in the capillary regime (Eq. 1), when the pressure inside the channel grows, its walls deform altering the shape of the cross-section hence the hydraulic diameter may grow and fall out of the limits dictated by Eq. (1). In these conditions, the PHS in straight vertical arrangement may work as a thermosyphon.

The performance of the PHS module inclined at 45° is comparable with the performance in vertical position, however one can observe a significant increase of the thermal resistance when the PHS module is in horizontal position. The maximum heating power is limited to about 50% of the value attained in the vertical position, because the evaporator temperature exceeds the value of 120°C, which cannot be sustained continuously by the material.

At the first step of the ascending heating power supply ramp (i.e., at stratup), the thermal resistance of the horizontal PHS module is even higher than the thermal resistance of the bare composite polypropylene sheet, which suggests the fluid transport between the evaporator and the condenser regions is not yet fully established, therefore there is some additional heat loss in the adiabatic zone. This can be partially explained with a significant drop of capillarity, which drives the condensate fluid back to the evaporator, due to the increase of temperature and pressure, which simultaneously reduce the surface tension and increase the hydraulic diameter, so that the system works in off-design conditions according to Eq. (1). According to Eq. (3), a heat loss in the adiabatic zone causes a reduction of the condenser temperature hence an increase of the apparent thermal resistance. When the same power supply at the evaporator is applied during the descending ramp, i.e., when the fluid transport is fully established, the thermal resistance is smaller than that of vacuumed PHS as expected.

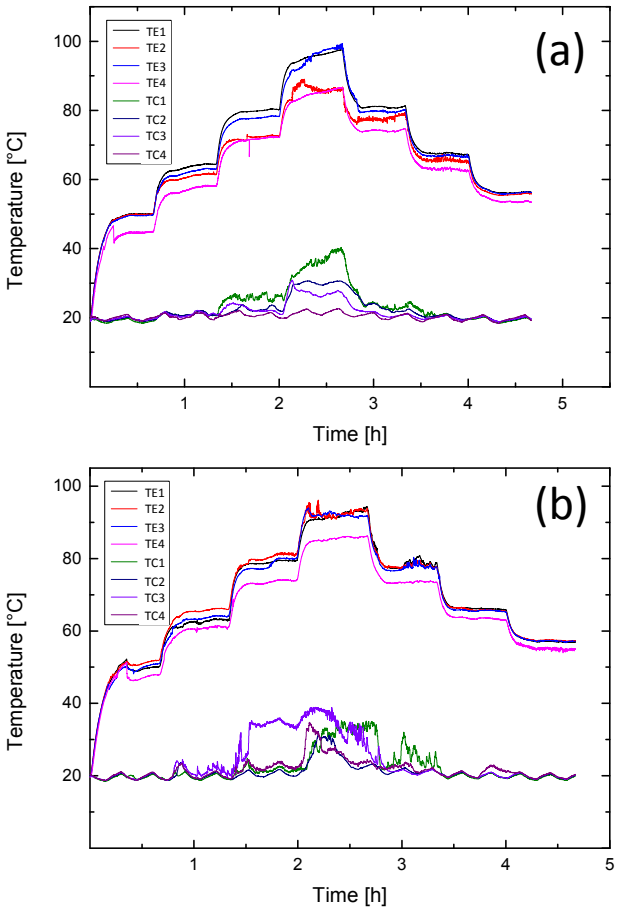

Fig. 12. Temperatures measured in the evaporator ($T_{E1} - T_{E4}$) and in the condenser ($T_{C1} - T_{C4}$) zones of the PHS in bent arrangement during the ascending/descending power supply ramp: (a) 45° bending; (b) 90° bending.

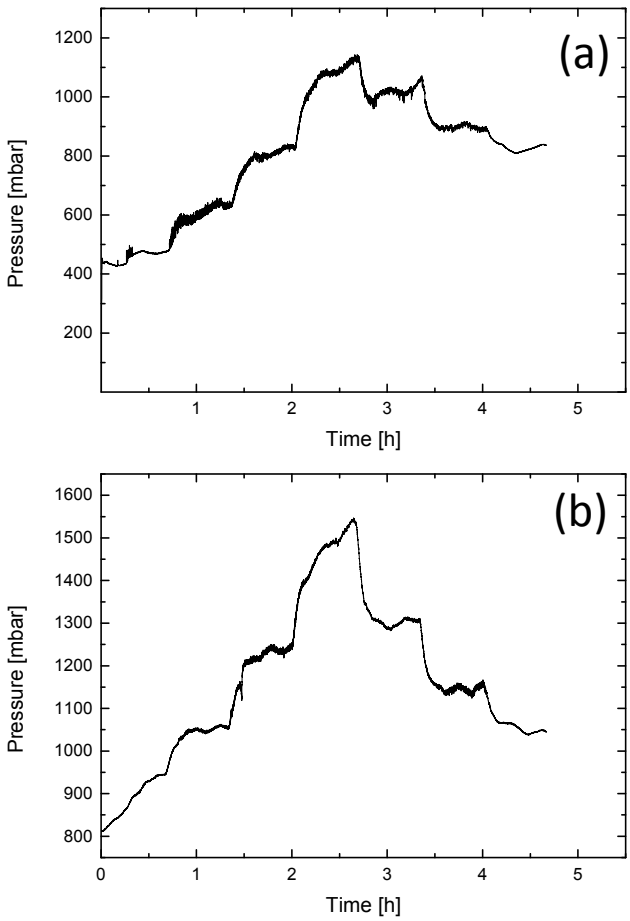

Fig. 13. Absolute pressure measured in the PHS in bent arrangement during the ascending/descending power supply ramp: (a) 45° bending; (b) 90° bending.

4.2 Bent Arrangement

Temperatures measured in the evaporator and in the condenser zones of the PHS in bent arrangement during the ascending/descending heat supply ramp are displayed in Figure 12, while the corresponding absolute pressure in the PHS channel is displayed in Figure 13.

The evaporator and condenser temperature trends appear qualitatively similar to those observed in the straight PHS, although it can be more difficult to achieve a pseudo-setady-state, especially at the higher values of thermal power supply. This is more evident from the pressure graphs (Figure 13).

The equivalent thermal resistance of the bent PHS is displayed in Figure 14 as a function of the thermal power supplied at the evaporator; at low power inputs ($\dot{Q} < 0.5\dot{Q}_{max}$), the performance of the bent PHS is 20% to 40% less than for the straight vertical PHS; at higher power inputs ($\dot{Q} > 0.5\dot{Q}_{max}$), the circulation is sufficiently sustained and the equivalent thermal resistances of the two arrangements become comparable.

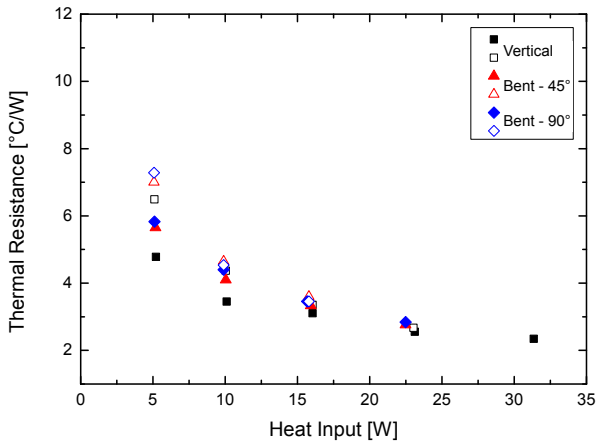

Fig. 14. Equivalent thermal resistance of the PHS in straight vertical and in bent arrangements, as a function of the heat rate supplied at the evaporator, for different bending angles; filled symbols: increasing power; open symbols: decreasing power. The standard deviation based on three tests is $\leq 8\%$.

5 Conclusions

A low-cost, flexible pulsating heat pipe was manufactured using three polypropylene sheets, bonded together by selective laser welding, where the central sheet contains the serpentine channel filled with the working fluid (FC-72). The thermal response was evaluated for different values of the heat input at the evaporator, for a number of different geometric configurations: straight (vertical, inclined at 45°, and horizontal), and bent at 45° and 90° in the adiabatic zone, with vertical evaporator and horizontal condenser. Initial results indicate a four-fold increase of the equivalent thermal conductance in comparison with that of the composite polymer constituting the heat pipe envelope. This suggests the proposed technology represents a promising route to produce composite polymeric materials with enhanced thermal performances.

Acknowledgements

O. Der gratefully acknowledges a YLSY doctoral studentship from the Republic of Turkey, Ministry of National Education. M. Marengo acknowledges the ESA MAP Project INWIP, the EPSRC HyHP Project (EP/P013112/1), and thanks Dr. D. Mangini, European Space Agency, for his experimental support and very useful discussions.

References

[1] Mameli, M., Marengo, M., and Khandekar, S., 2014. "Local heat transfer measurement and thermo-fluid characterization of a pulsating heat pipe". *International Journal of Thermal Sciencese,* **75**, pp. 140–152.

[2] Mameli, M., Manno, V., Filippeschi, S., and Marengo, M., 2014. "Thermal instability of a closed loop pulsating heat pipe: Combined effect of orientation and filling ratio". *Experimental Thermal and Fluid Science,* **59**, pp. 222–229.

[3] Manzoni, M., Mameli, M., de Falco, C., Araneo, L., Filippeschi, S., and Marengo, M., 2016. "Advanced numerical method for a thermally induced slug flow: application to a capillary closed loop pulsating heat pipe". *International Journal for Numerical Methods in Fluids,* **82**, pp. 375–397.

[4] Miyazaki, Y., 2005. "Cooling of notebook pcs by flexible oscillating heat pipes". In Proc. of ASME InterPACK Conference, San Francisco, USA.

[5] Maydanik, Y., Dmitrin, V., and Pastukhov, V., 2009. "Compact cooler for electronics on the basis of a pulsating heat pipe". *Appl. Thermal Eng.,* **29**, pp. 3511–3517.

[6] Rittidech, S., and Wannapakne, S., 2007. "Experimental study of the performance of a solar collector by closed-end oscillating heat pipe (ceohp)". *Applied Thermal Engineering,* **27**, pp. 1978–1985.

[7] Arab, M., Soltanieh, M., and Shafii, M., 2012. "Experimental investigation of extra-long pulsating heat pipe application in solar water heaters". *Experimental Thermal and Fluid Science,* **42**, pp. 6–15.

[8] Bliss, F., Clark, E., and Stein, B., 1970. *Construction and test of a flexible heat pipe*. American Society of Mechanical Engineers.

[9] Saaski, E. W., and Wright, J. P., 1975. "A flexible cryogenic heat pipe". In Fluid Mechanics and Heat Transfer, American Institute of Aeronautics and Astronautics, Thermophysics Conference, 10th, Denver, Colo.

[10] Wright, J., Brennan, P., and McCreight, C., 1976. "Development and test of two flexible cryogenic heat pipes". In Spacecraft Design, Testing and Performance, American Institute of Aeronautics and Astronautics, Thermophysics Conference, 11th, San Diego, CA.

[11] Odhekar, D. D., and Harris, D. K., 2011. "Bendable heat pipes using sintered metal felt wicks". *Frontiers in Heat Pipes,* **2**, pp. 1–8.

[12] McDaniels, D., and Peterson, G. P., 2001. "Investigation of polymer based micro heat pipes for a flexible spacecraft radiator". In Spacecraft Design, Testing and Performance, 2001 ASME International Mechanical Engineering Congress and Exposition, New York, NY, United states.

[13] Oshman, C., Shi, B., Li, C., Yang, R., Peterson, G. P., and Bright, V. M., 2011. "The development of polymer-based flat heat pipes". *Journal of Microelectromechanical Systems,* **20**, pp. 410–417.

[14] Oshman, C., Li, Q., Liew, L.-A., Yang, R., Bright, V. M., and Lee, Y. C., 2013. "Flat flexible polymer heat pipes". *Journal of Micromechanics and Microengineering,* **23**, pp. 1–6.

[15] Lim, J., and Kim, S. J., 2018. "Fabrication and experimental evaluation of a polymer-based flexible pulsating heat pipe". *Energy Conversion and Management,* **156**, pp. 358 – 364.

[16] Der, O., Marengo, M., and Bertola, V., 2018. "A low-cost, flexible pulsating heat pipe technology". In Proc. 3rd Thermal and Fluids Engineering Conference (TFEC), Fort Lauderdale (USA).

[17] Acherjee, B., Arunanshu S. Kuar, S. M., and Misra, D., 2015. "Laser transmission welding of polycarbonates: experiments, modeling, and sensitivity analysis". *The International Journal of Advanced Manufacturing Technology,* **78**, pp. 853–861.

[18] Liu, H., Jiang, H., Chen, G., Guo, D., Yan, Z., Li, P., and Wang, X., 2016. "Investigation on the laser transmission weldability and mechanism of the graft-modified polyethylene and pa66". *The International Journal of Advanced Manufacturing Technology,* **86**, pp. 809–816.

[19] Paudel, S. B., and Michna, G. J., 2014. "Effect of inclination angle on pulsating heat pipe performance". In Proc. ASME 2014 12th International Conference on Nanochannels, Microchannels and Minichannels, Chicago, Illinois (USA).

[20] Gere, J., 2004. *Mechanics of Materials*. Brooks/Cole–Thomson Learning.